INTERNATIONAL JOURNAL OF ENGINEERING MANAGEMENT SCIENCE
journal homepage: www.ijems.online/index.php/ijems/index

Mechanical and Tribological Performance of Aramid Fiber-Reinforced Photopolymer Composites Fabricated via Stereolithography for Sustainable Bearing Applications

R Raghavendra[1*] & Dr. M.K Aravindan[2]

[1]Student, M. Tech, Department of Mechanical Engineering, Jain Deemed to Be University, Bengaluru, India.

[2]Associate Professor, Department of Mechanical Engineering, Jain Deemed to be University, Bengaluru, India.

***Corresponding E-mail:** raghavendraraju6732@gmail.com

Received: 5-4-2026 ***Revised: 15-4-2026*** ***Accepted: 5-5-2026***

Keyword

Aramid Fiber;
Stereolithography (SLA);
Polymer Composite;
Tribological Performance;
Sustainable Bearing Materials.

Abstract

This study examines the mechanical and tribological behavior of aramid fiber reinforced polymer (AFRP) composites made through Stereolithography (SLA) additive manufacturing intended for sustainable bearing applications. The polymer matrix used was SLA photo curable resin which was reinforced with aramid fibers at weight fractions of 0.25 wt% and 0.50 wt%. Tensile testing was done as per ASTM D638 and Shore D hardness was evaluated following ASTM D2240. Pin on disc tribological testing was carried out according to ASTM G99 against an EN31 hardened steel counterface under dry sliding conditions. Results show that adding aramid fibers progressively improves tensile strength and surface hardness over the unreinforced SLA resin baseline. Among the tested compositions the 0.50 wt% composite recorded the highest tensile strength and hardness values. The same composition also showed a substantially reduced coefficient of friction and wear loss across different loads and speeds. Frictional heat generation was also found to decrease in the composites which supports the possibility of reduced lubrication requirements in practical bearing applications.

1. Introduction:

Modern engineering systems require advanced materials that are lightweight and mechanically strong with minimal maintenance needs. In motion based systems like bearings and gears tribological performance directly controls system efficiency and operational life. The growing demand for energy efficient and sustainable mechanical systems has pushed researchers to look for alternatives that can outperform conventional metallic and polymer based components. Traditional metallic bearings are heavy and corrosion prone and need continuous lubrication to work reliably. Their manufacturing and operational lifecycle also adds significantly to carbon emissions and industrial waste. These issues have driven global research interest in composite materials that offer better tribological behavior with lower environmental impact [1,2].

Fiber reinforced polymer (FRP) composites are well suited for bearing applications because of their high specific strength and corrosion resistance and damping characteristics and potential for self lubrication. Their structure of strong fibers embedded in a polymer matrix allows efficient load distribution and controlled frictional behavior under sliding contact. The type of reinforcing fiber plays a major role in determining the

final composite properties. Aramid fibers known commercially as Kevlar stand out for their tensile strength to weight ratio and abrasion resistance and thermal stability and impact absorption. These properties have led to their use in aerospace panels and ballistic armor and automotive friction pads [3,4,5].

When aramid fibers are embedded in a polymer matrix the composite shows improved load carrying capacity and resistance to material removal at sliding interfaces. The hydrogen bonding within aramid fiber molecules promotes good interfacial adhesion with the matrix and helps stress transfer during dynamic loading. From a tribological standpoint aramid fibers at the sliding interface promote transfer film formation on the counterface which reduces abrasive wear and lowers the coefficient of friction (COF) over extended operation [6,7]. These advantages make aramid fiber reinforced polymer (AFRP) composites good candidates for replacing conventional bearing materials in industrial and automotive applications.

The fabrication method used to produce composite bearings has a strong influence on their microstructural integrity and functional performance. Conventional methods like hand lay up and compression molding have limitations in geometric complexity and dimensional accuracy and reinforcement uniformity. Additive Manufacturing (AM) has changed composite development by enabling precise layer by layer fabrication of complex geometries with minimal material wastage. Among AM technologies Stereolithography (SLA) is particularly suited for polymer composites because of its laser driven photopolymerization which provides dimensional accuracy and good surface finish and consistent layer bonding [8,9].

SLA allows fiber reinforcements to be incorporated into photocurable resins before printing which enables fabrication of AFRP composites with homogeneous microstructures that are hard to achieve through conventional molding. The UV laser curing in SLA ensures complete resin infiltration around fiber surfaces and promotes strong interfacial bonding that is important for stress transfer and wear resistance. The smooth surface quality of SLA printed components is also beneficial for tribological applications where surface roughness directly affects frictional response and initial wear rate [10,11].

Sustainability has become increasingly important in material selection in modern engineering. Composite bearings offer sustainability advantages because their lower density reduces the mass of mechanical assemblies and decreases energy demands during operation. Their improved wear resistance extends component service life and reduces replacement frequency. AFRP composites can also operate under dry or minimally lubricated conditions because of the tribological benefits of aramid fibers which reduces the use of lubricants that pose environmental risks [5,6]. SLA further contributes to sustainability by minimizing material scrap and supporting near net shape production which reduces energy and raw material requirements [12].

Kausar and Siddiq [1] showed that epoxy composites reinforced with modified multi walled carbon nanotube coated aramid fibers have markedly improved tensile strength and glass transition temperature compared to unmodified aramid epoxy laminates. The study confirmed that interfacial engineering at the fiber matrix boundary is critical for composite performance improvements and that proper fiber surface functionalization enhances filler distribution and mechanical response.

Park and Jang [2] studied the impact behavior of four layer aramid glass fiber hybrid laminates and found that stacking sequence and fiber surface treatment significantly affect energy absorption and delamination behavior. Positioning aramid layers on the tension bearing face increases total impact energy absorption which is useful for designing bearing components that must withstand impact loading. Liu et al. [3] developed microwave cured carbon aramid fiber epoxy sandwich composite patches for structural repair of cracked aluminum alloy plates and found that three layer carbon aramid configurations recover approximately 86% tensile capacity and 190% bending performance of undamaged plates.

Karataş [7] studied the friction performance of AFRP composites under ball on disc sliding at loads of 8 N and 12 N and speeds of 300 to 550 rpm. The study found that AFRP composites maintain a stable coefficient of friction under moderate loads and that specimen A1 showed a 287.5% lower wear related value at 8 N compared to 12 N which shows strong sensitivity of tribological performance to contact pressure.

Lu et al. [8] developed graphene oxide aramid nanofiber paper based self lubricating composites for aerospace bearing liner applications. At 1 wt% graphene oxide loading the composite achieved reductions in coefficient of friction and volumetric wear rate of approximately 23% and 89% respectively relative to graphene oxide free samples. Sudheer et al. [9] evaluated wear performance of Kevlar aramid fiber reinforced epoxy composites modified with ceramic potassium titanate whisker nano powders using Taguchi design and found that sliding distance was the most influential factor governing specific wear rate followed by velocity and load and powder content.

Yu et al. [11] studied high temperature tribological behavior of self lubricating fabric composites reinforced with polyimide and PEEK and aramid fibers at 163°C. Polyimide composites achieved the lowest wear rate of approximately 1.29×10^{-8} mm³/(N·mm) and the study showed that fiber rigidity and thermal stability are critical for tribological durability at elevated temperatures. Han et al. [12] found that 3 phr aramid loading in silica filled rubber compounds provides optimal improvement in silica dispersion and enhanced silanization degree which underlines the broad applicability of aramid fibers across diverse polymer systems.

Despite accumulated knowledge on aramid fiber composites and SLA based polymer manufacturing significant gaps remain in the literature regarding their combined application for tribological component development. Existing studies on SLA processed composites mostly use glass fiber or carbon fiber or particulate reinforcements with very limited attention on aramid fiber variants. Most tribological investigations on aramid composites also rely on conventional molding techniques that introduce processing variabilities absent in SLA fabrication. Direct benchmarking of SLA printed AFRP composites against conventional bearing materials under standardized dry sliding conditions with simultaneous measurement of friction and wear rate and surface degradation mechanisms has not been adequately addressed.

The effect of SLA process parameters on fiber distribution uniformity and its influence on tribological performance also remains unexplored. The potential of AFRP SLA composites to reduce lubrication requirements and minimize frictional heat generation and extend operational service life under realistic bearing conditions has not been systematically evaluated. Quantitative energy consumption analysis comparing AFRP SLA bearings with metallic counterparts under equivalent loading conditions is also absent from the literature. These research gaps form the primary motivation for this investigation which aims to characterize the mechanical and tribological performance of SLA fabricated aramid fiber reinforced polymer composites and validate their viability as sustainable alternatives in motion based engineering systems requiring low friction and minimal maintenance and extended service durability.

2. Materials and Methods

2.1 Materials

The experimental work used two main constituent materials. A commercial photocurable SLA resin was used as the matrix phase and chopped aramid fibers served as the reinforcing phase. The SLA resin was a standard photo curable liquid resin supplied for desktop SLA printing systems. It showed good photopolymerization response and dimensional fidelity after curing and reasonable compatibility with short fiber reinforcements. The resin also has a refractive index and light transmittance profile that supports layer by layer UV curing without excessive laser scattering from embedded fibers. Aramid fibers of Kevlar® 29 grade were procured in continuous tow form and then chopped to uniform micro lengths of approximately 100 to 200 μm using precision scissors and a fiber milling approach. Chopping to short lengths is necessary to keep adequate suspension in the liquid resin and to prevent nozzle clogging or print head interference during the SLA resin vat replenishment cycle. Key properties of both constituent materials are listed in Table 1. The EN31 steel disc used as the tribological counterface was separately procured and precision machined to 60 HRC hardness and Ra ≤ 0.5 μm surface roughness to represent standardized metallic bearing shaft conditions.

Table 1. Properties of constituent materials used in composite fabrication

Property	SLA Photopolymer Resin	Aramid Fiber (Kevlar® 29)
Density (g/cm³)	1.16	1.44
Tensile Strength (MPa)	38–45	2,900–3,600
Elastic Modulus (GPa)	2.5–3.0	70–83
Elongation at Break (%)	6–8	3.6–4.0
Shore-D Hardness	78–82	—
Thermal Stability (°C)	Up to 110	Up to 430

2.2 Composite Formulation and Designation

Three composite variants were prepared for this study. A neat SLA resin control specimen was designated as C0 and two fiber reinforced composites were made with 0.25 wt% aramid fiber (C1) and 0.50 wt% aramid fiber (C2). This formulation approach was chosen to find the performance threshold of reinforcement without affecting resin processability or SLA print quality. Higher fiber loadings were not considered in this study. Preliminary trials showed increased viscosity and poor print quality above 0.50 wt% which is consistent with findings from similar studies on short fiber filled SLA resins. The composite designation scheme is given in Table 2.

Table 2. Composite designation and formulation details

Designation	Matrix	Aramid Fiber (wt%)
C0	SLA Resin	0
C1	SLA Resin	0.25
C2	SLA Resin	0.50

2.3 Composite Preparation Procedure

Before mixing aramid fibers were dried in a circulating air oven at 80°C for 2 hours to remove absorbed moisture that could introduce void nucleation sites during photopolymerization. The required fiber mass was then gradually added into the measured volume of liquid SLA resin under continuous magnetic stirring at 300 rpm for 45 minutes. The rotation speed was kept at a level that gives adequate shear for fiber wetting without causing fiber breakage. Mixing temperature was maintained at ambient conditions of 25 ± 2°C to avoid premature partial curing or excessive viscosity increase.

After mechanical stirring the resin fiber mixture was subjected to vacuum degassing at −95 kPa for 15 minutes to remove entrapped air bubbles that could create porosity defects within printed layers. The degassed mixture was then allowed to rest for 5 minutes before being transferred into the SLA printer resin vat.

Vacuum degassing is important for tribological specimen quality because sub surface voids act as stress concentration sites that speed up crack initiation under sliding contact loads.

The entire mixing and degassing procedure was consistently repeated for all composite formulations to ensure reproducibility across specimen batches.

2.4 SLA Fabrication Process and Parameters

All specimens were fabricated using a desktop SLA printer with a 405 nm UV laser source. CAD models for tensile specimens as per ASTM D638 and hardness flat rectangular slabs and tribological cylindrical pins of 8 mm diameter × 25 mm height were created in SolidWorks and exported in STL format. The STL files were then imported into the printer slicing software where print parameters were optimized based on the altered photopolymerization kinetics of fiber filled resin. The optimized SLA process parameters are listed in Table 3.

After fabrication all specimens were removed from the build platform and rinsed in isopropyl alcohol (IPA) for 5 minutes to remove uncured resin surface residues. They were then subjected to additional UV post curing at 60°C for 30 minutes in a dedicated post cure chamber. Post curing ensures complete photopolymer cross linking which maximizes mechanical stiffness and wear resistance.

Specimens were measured using a digital vernier caliper with a resolution of 0.01 mm to verify dimensional conformance with target geometries before proceeding to mechanical and tribological testing.

Table 3. SLA fabrication process parameters

Parameter	Value
Laser wavelength (nm)	405
Layer thickness (μm)	50
Exposure time per layer (s)	8
Laser scan speed (mm/s)	250
Build orientation	Vertical (Z-axis)
Post-cure UV exposure (min)	30
Post-cure temperature (°C)	60

2.5 Specimen Design and Standards

All test specimens were designed and fabricated following recognized ASTM international standards to ensure result validity and reproducibility. Tensile specimens followed ASTM D638 Type I geometry with an overall length of 165 mm and gauge length of 57 mm and gauge width of 13 mm.

Hardness evaluation specimens were prepared as flat rectangular slabs of 70 × 25 × 6 mm as per ASTM D2240 requirements. Tribological pin specimens were fabricated as cylindrical pins of 8 mm diameter and 25 mm length for ASTM G99 pin on disc testing.

A minimum of five specimens per composite variant per test type were fabricated to allow statistical analysis of results and to report mean values with standard deviation.

Table 4 gives a summary of specimen geometry and testing standards.

Table 4. Summary of specimen geometry and testing standards

Test Type	Standard	Specimen Geometry
Tensile	ASTM D638 Type I	Dog-bone, 165 mm length
Hardness	ASTM D2240 (Shore-D)	Flat slab, 10×15×10 mm
Friction & Wear	ASTM G99	Cylinder pin, Q8×25 mm

2.6 Mechanical Testing

Tensile testing was done using a servo controlled Universal Testing Machine (UTM) with a 5 kN load cell at a crosshead speed of 2 mm/min following ASTM D638. Load displacement data was continuously acquired and converted to engineering stress strain curves. From these curves ultimate tensile strength (UTS) and Young's modulus of elasticity and percentage elongation at break were calculated.

Shore D hardness was evaluated using a calibrated Shore D Durometer with a standard 1.25 mm diameter truncated cone indenter applied perpendicularly to the flat specimen surface with 1 kg standard load held for 1 second. Five measurements were taken at different locations on each specimen surface and averaged to reduce local microstructural bias.

2.7 Tribological Testing

Tribological evaluation was carried out using a pin on disc tribometer (TR-20LE Ducom Instruments India) under dry sliding conditions as per ASTM G99. The composite cylindrical pin was pressed against a rotating EN31 steel disc of 60 HRC hardness and Ra ≤ 0.4 μm surface roughness.

Testing was done under three normal load levels of 10 N and 20 N and 30 N and sliding speeds of 100 rpm and 200 rpm and 300 rpm with a track radius of 40 mm for a total sliding distance of 1000 m per run.

The coefficient of friction (COF) was continuously recorded by the tribometer's integrated strain gauge load cell. Specimen mass was measured before and after each test using a precision analytical balance.

3. Results and Discussion

3.1 Tensile Properties

Tensile test results for the three composite variants are presented in Fig.1 and Fig.2 and are discussed with respect to the influence of aramid fiber reinforcement on load transfer efficiency and fracture behavior. The neat SLA resin (C0) showed a tensile strength of 33.2 MPa with an elongation at break of 3.9% which is typical for photopolymer resins fabricated via stereolithography. When 0.25 wt% aramid fiber was added (C1) tensile strength increased to 42.6 MPa which is an improvement of approximately 28.3% over the unreinforced resin and elongation at break decreased to 2.8%.

Further addition of aramid fiber to 0.50 wt% (C2) gave a tensile strength of 51.4 MPa which corresponds to an overall improvement of 54.8% relative to C0 and elongation at break reduced further to 1.9%.

The progressive increase in tensile strength with fiber content is attributed to the high intrinsic strength and stiffness of aramid fibers and their effective stress transfer capability within the SLA resin matrix. The SLA process enables precise curing and relatively uniform fiber dispersion which improves interfacial bonding and minimizes defects like voids or fiber pullout. This load sharing mechanism allows the applied stress to be transferred from the polymer matrix to the reinforcing fibers thereby improving the overall composite strength [13-16]. These findings are in agreement with the reinforcement mechanisms reported by Kausar and Siddiq [1] where enhanced interfacial interactions significantly improved tensile performance in fiber reinforced polymer systems.

A reduction in elongation at break is noted with increasing fiber content which indicates a transition from ductile to more brittle behavior. Rigid aramid fibers restrict polymer chain mobility and limit plastic deformation under tensile loading. This trade off between strength and ductility is characteristic of short fiber reinforced composites and has been widely reported in the literature [3]. The reduced elongation suggests that failure in reinforced composites occurs at lower strain levels because of stress concentration at the fiber matrix interface and reduced matrix continuity.

The overall tensile response shows that while aramid fiber reinforcement significantly improves strength it also reduces deformability. This balance between increased load bearing capacity and decreased ductility must be carefully considered in bearing component applications where both strength and toughness are important [17-20].

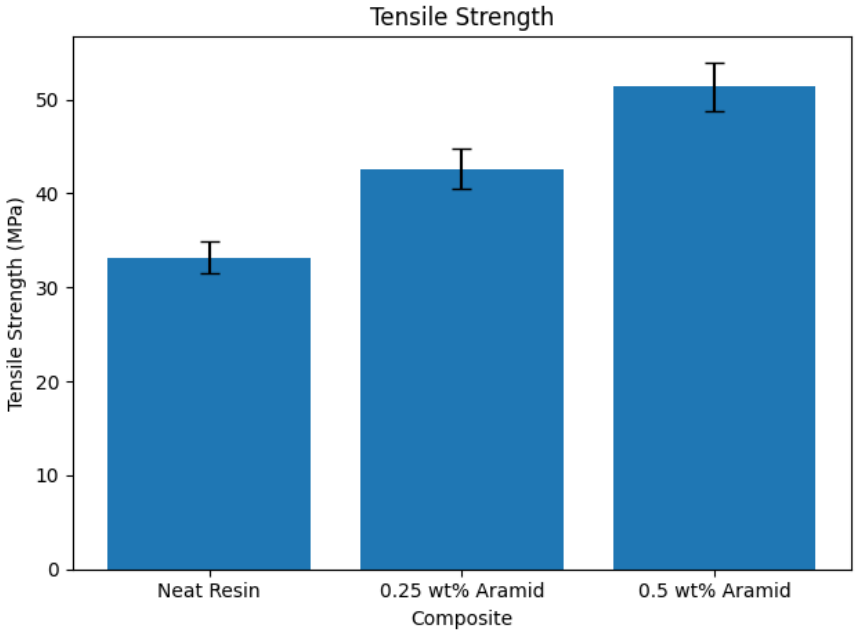

Fig.1: Effect of aramid fibre content on Tensile Strength

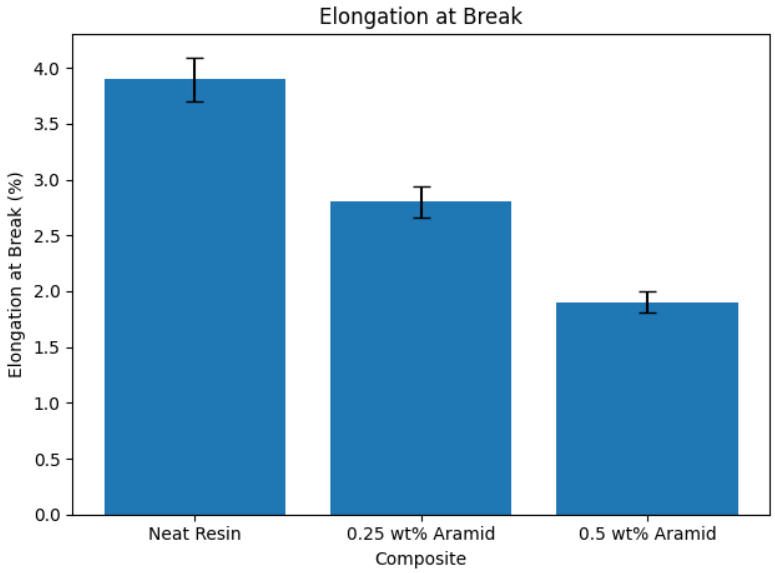

Fig.2: Effect of aramid fibre content on ductility

3.2 Shore-D Hardness

Shore D hardness results for all composite variants are presented in Fig.3. The neat resin (C0) showed a baseline hardness of 74 HD which represents the inherent resistance of the SLA fabricated photopolymer to localized surface deformation. Adding 0.25 wt% aramid fiber (C1) increased hardness to 79 HD which is an improvement of approximately 6.8% over the neat resin. Further addition to 0.50 wt% aramid fiber (C2) gave a hardness value of 83 HD representing an overall improvement of about 12.2% relative to C0.

The increase in hardness with fiber content shows that aramid fiber reinforcement effectively improves resistance to indentation and surface deformation. This is mainly because of the high stiffness and load bearing capability of aramid fibers which restrict localized deformation under the indenter. Fibers within the polymer matrix reduce chain mobility and distribute the applied load more evenly resulting in a harder composite surface. Uniform fiber dispersion achieved through the SLA process also contributes to consistent hardness improvement by reducing weak regions within the material [18-22].

Harder surfaces offer greater resistance to abrasive wear by limiting asperity penetration and reducing micro cutting during sliding contact. The improved hardness in reinforced composites is therefore expected to contribute directly to reduced wear rates and better durability in applications involving repeated contact or sliding motion [22-25]. Similar trends were reported by Karataş [7] who found that aramid fiber reinforced polymer composites show improved surface integrity and resistance to deformation under mechanical loading.

Overall the results confirm that even low weight fractions of aramid fiber noticeably improve the surface hardness of SLA fabricated composites and enhance their suitability for applications requiring resistance to wear and surface damage.

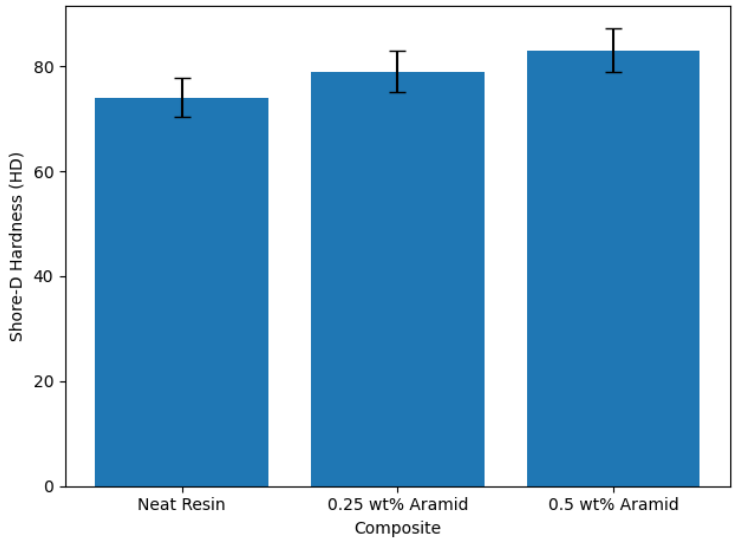

Fig.3: Effect of aramid fibre content on hardness

3.3 Tribological Performance: Coefficient of Friction

The coefficient of friction (COF) was evaluated under varying normal loads of 10 N and 20 N and 30 N and different sliding speeds and the results are shown in Fig.4. The neat resin (C0) showed relatively high COF values of 0.48 and 0.55 and 0.62 at 10 N and 20 N and 30 N respectively which indicates poor tribological performance under dry sliding conditions. The increase in COF with applied load is typical of polymer metal contact where higher normal forces promote increased asperity interaction and adhesive friction.

Adding aramid fibers reduced COF noticeably across all load conditions. The 0.25 wt% aramid fiber composite (C1) showed COF values of 0.36 and 0.42 and 0.51 at 10 N and 20 N and 30 N which correspond to reductions of approximately 25.0% and 23.6% and 17.7% respectively compared to the neat resin. The 0.50 wt% composite (C2) showed the lowest COF values of 0.20 and 0.34 and 0.44 at the respective loads corresponding to reductions of 58.3% and 38.2% and 29.0% relative to C0.

The reduction in COF with increasing aramid fiber content is due to the self lubricating nature of the fibers and the formation of a stable transfer film on the steel counterface during sliding. This transfer film acts as a low shear interfacial layer that reduces direct contact between the polymer matrix and the metallic surface and minimizes adhesive friction. Similar tribofilm assisted friction reduction was reported by Lu et al. [8] in aramid based composite systems.

Despite the overall reduction in COF an increasing trend with load is observed for all materials. At higher loads contact pressure increases which can disrupt the continuity of the transfer film and expose fresh material to the counterface leading to increased friction. This is consistent with findings by Karataş [7] who reported increased frictional response in aramid fiber reinforced composites at elevated loads due to intensified surface interactions.

The effect of sliding speed on COF was also studied at a constant load of 10 N. At 100 rpm the COF values for C0 and C1 and C2 were 0.48 and 0.36 and 0.20 respectively which matches the baseline values seen under low speed conditions (Fig.5). As sliding speed increased to 200 rpm COF values decreased to 0.456 and 0.342 and

0.190 and further reduced to 0.432 and 0.324 and 0.180 at 300 rpm. This represents a gradual reduction of approximately 5 to 10% with increasing speed for all composites.

The decrease in COF with sliding speed is attributed to better formation and stability of the transfer film at higher velocities which reduces adhesive interactions and promotes smoother sliding. Increased sliding speed may also lead to localized thermal softening at the interface which further reduces frictional resistance. Reinforced composites particularly C2 showed more stable and consistently lower COF values across the speed range which indicates better tribological performance under varying operating conditions.

Overall aramid fiber reinforcement significantly improves frictional behavior under both varying load and sliding speed conditions making these composites suitable for applications requiring reduced friction and better wear performance under dynamic contact environments.

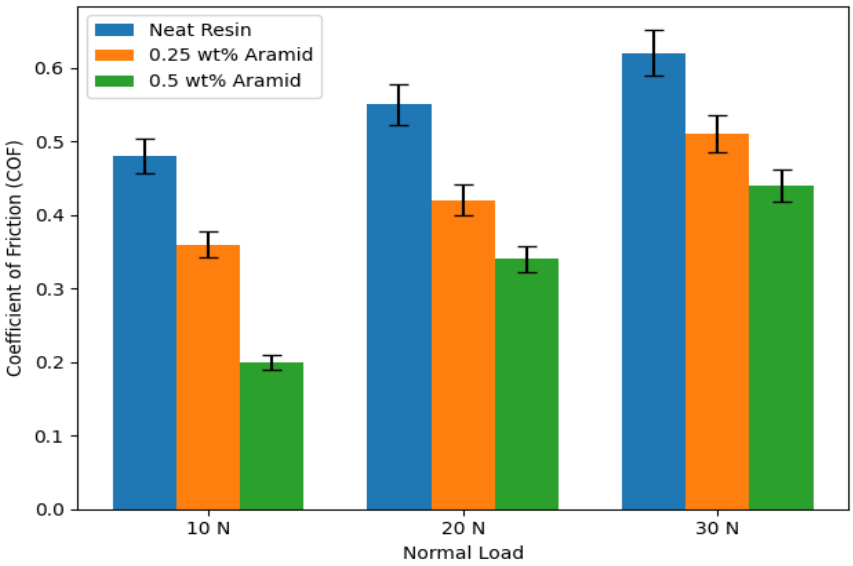

Fig.4: Effect of aramid fibre content on COF at different loads

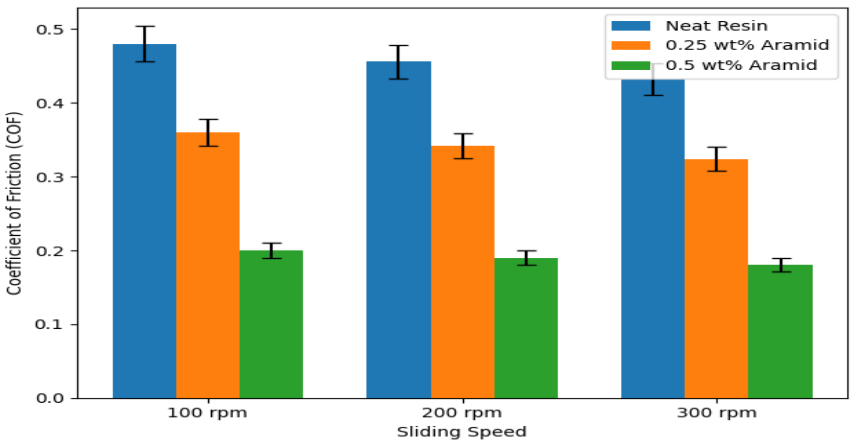

Fig. 5: Effect of aramid fibre content on COF at different sliding speeds

3.4 Wear Performance

Wear behavior of the composites was evaluated in terms of weight loss and the results under different normal loads are presented in Fig.6. The neat resin (C0) showed weight losses of 0.578 mg and 1.476 mg and 3.035 mg at 10 N and 20 N and 30 N respectively which confirms the high susceptibility of unreinforced photopolymer

to material removal under dry sliding conditions. The progressive increase in weight loss with load indicates intensified contact severity and increased material detachment at higher normal forces.

Adding 0.25 wt% aramid fiber (C1) reduced weight loss noticeably to 0.389 mg and 1.046 mg and 2.203 mg at the respective loads. These correspond to reductions of approximately 32.7% and 29.1% and 27.4% compared to the neat resin. The 0.50 wt% composite (C2) showed the lowest weight loss values of 0.250 mg and 0.730 mg and 1.753 mg which represent reductions of 56.7% and 50.5% and 42.2% relative to C0.

The reduction in weight loss with increasing aramid fiber content is due to several synergistic mechanisms. The high abrasion resistance of aramid fibers acts as a protective barrier that shields the polymer matrix from direct interaction with hard steel asperities. The increased hardness of the composite also reduces penetration depth and limits micro cutting and plowing mechanisms. Formation of a stable tribological transfer film on the counterface further reduces effective contact area and minimizes material removal.

The effect of sliding speed on wear behavior was also studied at a constant load of 10 N and the corresponding weight loss values are given in Table 8. For the neat resin (C0) weight loss increased from 0.578 mg at 100 rpm to 1.157 mg at 200 rpm and further to 1.735 mg at 300 rpm which shows a near linear increase with sliding speed (Fig.7). A similar trend was seen for reinforced composites where C1 showed weight losses of 0.389 mg and 0.778 mg and 1.166 mg and C2 showed 0.250 mg and 0.499 mg and 0.749 mg at 100 and 200 and 300 rpm respectively.

The increase in weight loss with sliding speed is mainly because of the increased sliding distance and higher cumulative interaction between contacting surfaces which accelerates material removal. Higher speeds can also lead to localized temperature rise at the interface which weakens the matrix and promotes wear. Despite this increase reinforced composites consistently showed significantly lower weight loss compared to neat resin across all speeds which demonstrates improved wear resistance under dynamic operating conditions.

These observations are consistent with findings of Sudheer et al. [9] who identified sliding distance as a dominant parameter influencing wear behavior in fiber reinforced polymer composites. The present results further confirm that increasing sliding severity through higher load or speed leads to progressive degradation of the protective transfer film and increased matrix exposure. The transition from moderate wear at 10 N to severe wear at 30 N in neat resin highlights the absence of reinforcement whereas AFRP composites maintain controlled wear progression because of effective load distribution and fiber reinforcement.

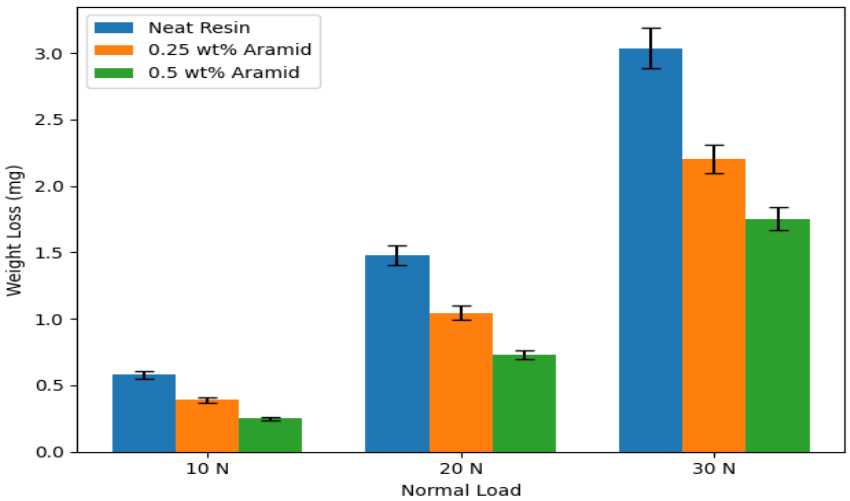

Fig. 6: Variation of wear loss with loads

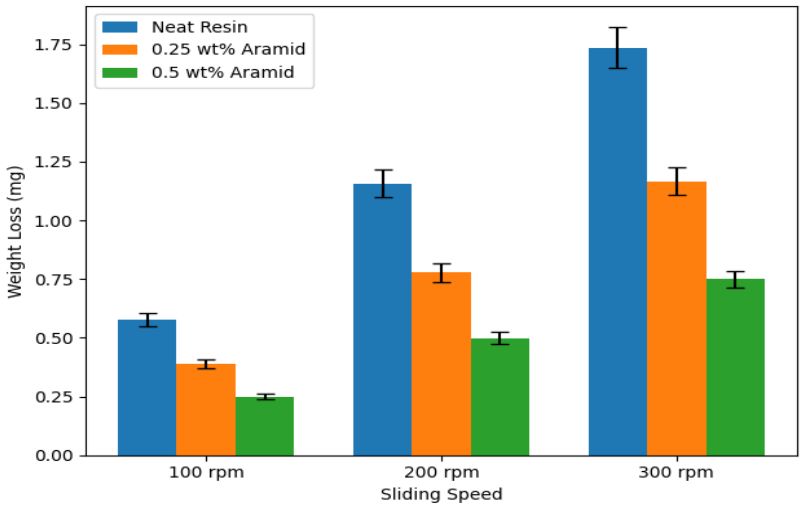

Fig. 7: Variation of wear loss with sliding speeds

4. Conclusions

- The following conclusions are drawn from the experimental investigation of SLA fabricated aramid fiber reinforced polymer composites.
- Aramid fiber reinforcement significantly improves mechanical performance. The 0.50 wt% composite (C2) achieved a tensile strength of 51.4 MPa which is a 54.8% increase over neat resin and a Shore D hardness of 83 HD which is a 12.2% improvement. This confirms that even low fiber loadings effectively improve structural integrity though reduced elongation indicates increased brittleness.
- Tribological performance improved noticeably with fiber addition. C2 showed the lowest coefficient of friction values of 0.20 and 0.34 and 0.44 at 10 N and 20 N and 30 N respectively. These correspond to reductions of up to 58.3% at 10 N compared to neat resin which demonstrates the strong friction reducing capability of aramid fiber through transfer film formation.
- Wear resistance evaluated in terms of weight loss showed substantial improvement. C2 achieved reductions of 56.7% and 50.5% and 42.2% at 10 N and 20 N and 30 N respectively. This highlights the effectiveness of aramid fibers in minimizing material removal through abrasion resistance and increased hardness and tribofilm formation.
- Both load and sliding speed significantly influence tribological behavior. Weight loss increased and COF generally rose with load while sliding speed caused a moderate increase in wear but a slight reduction in COF of around 8%. This indicates the combined role of contact severity and transfer film stability in governing performance.
- Sliding speed variation showed a proportional increase in weight loss with increasing rpm where values approximately doubled at 200 rpm and tripled at 300 rpm compared to 100 rpm. COF decreased slightly across all composites which shows that higher speeds improve transfer film formation but also increase cumulative wear due to extended sliding interaction.
- SLA fabricated AFRP composites show strong potential for bearing applications. The combination of reduced friction and improved wear resistance and enhanced surface hardness provides a lightweight and efficient alternative to conventional materials with fiber reinforcement ensuring stable performance under varying operational conditions.

5. Conflict of Interest

The authors declared that no potential conflicts of interest concerning the research, authorship, and/or publication of this article.

6. Plagiarism Policy

The authors declare that any kind of violation of plagiarism, copyright, and ethical matters will be handled by all authors. Journalists and editors are not liable for the aforesaid matters.

7. Sources of Funding

The authors received no financial aid to support the study.

References:

[1] Kausar, A., & Siddiq, M. (2016). Epoxy composites reinforced with multi-walled carbon nanotube/poly(ethylene glycol) methylether-coated aramid fiber. Journal of Polymer Engineering, 36(5), 465–471.

[2] Park, R., & Jang, J. (2001). Impact behavior of aramid fiber/glass fiber hybrid composite: Evaluation of four-layer hybrid composites. Journal of Materials Science, 36, 2359–2367.

[3] Liu, X., Wu, J., Xi, J., & Yu, Z. (2019). Bonded repair optimization of cracked aluminum alloy plate by microwave cured carbon-aramid fiber/epoxy sandwich composite patch. Materials, 12, 1655.

[4] Nam, J., Kim, G., Kim, H., Jeon, J., & Shinohara, Y. (2015). Damage evaluation of aramid fiber reinforced cement composites by high velocity impact. Asian Journal of Chemistry, 27(11), 4266–4270.

[5] Stojanović, D. B., Obradović, V., Bajić, D., & Uskoković, P. S. (2024). A new generation of aramid fibers/poly(vinyl butyral) composites for ballistic protection: Recent development and advances. Journal of Engineered Fibers and Fabrics, 19, 1–22.

[6] Overberg, M., Khurshid, M. F., Abdkader, A., Hasan, M. M. B., & Cherif, C. (2024). Development of a micro-scale hybridized yarn structure from recycled carbon, aramid and polyamide 6 staple fibers for thermoplastic composites with improved impact strength. Textile Research Journal, 94(5–6), 636–648.

[7] Karataş, M. A. (2021). Investigation of friction performance and surface integrity of aramid fiber-reinforced polymer matrix composite. Polymer Composites, 42(12), 6349–6361.

[8] Lu, Y., Zhang, Y., Wang, Q., Wang, H., & Gao, G. (2025). Tribological properties of graphene oxide reinforced aramid paper-based composites. Tribology International, 202, 110296.

[9] Sudheer, M., Kamath, B. R., Yadav, R. Y., Pai, G. S., & Vishwanath, A. (2025). Wear performance of polymer matrix composites reinforced with aramid fibers and modified with ceramic nano-powders. Journal of Environmental Nanotechnology, 14(2), 182–188.

[10] Hashimoto, A., Satoh, M., & Iwasalu, T. (2003). Effect of morphology of fiber on mechanical properties of short fiber–powder composite. Journal of the Society of Materials Science, Japan, 52(1), 95–100.

[11] Yu, M., Zhang, M., Fang, L., Ren, M., Liang, L., Xie, W., & Ma, P. (2022). Wear failure mechanism analysis of self-lubricating fabric composites at high temperature. Journal of Industrial Textiles, 52, 1–17.

[12] Han, D., Ma, Q., Wang, J., Chen, H., Wang, C., & Han, W. (2022). Effect of the addition of different amounts of aramid fibers on metal friction and wear during mixing. Polymers, 14, 2961.

[13] Vinay, D. L., Keshavamurthy, R., & Ugrasen, G. (2024). Tribological characteristics of copper powder-reinforced PLA composites fabricated via FDM. Interactions, 245(1), 181.

[14] Vinay, D. L., Keshavamurthy, R., & Ugrasen, G. (2024). Tensile characteristics of metal-filled 3D printed PLA-based polymer composites. Interactions, 245(1), 154.

[15] Kumar, N. H., Adarsha, H., Keshavamurthy, R., & Kapilan, N. (2024). Influence of carbon nanofibre addition on mechanical behaviour of PLA-based 3D printed polymer nanocomposites. Journal of the Institution of Engineers (India): Series D, 105(1), 33–47.

[16] Kumar, G. S. P., Keshavamurthy, R., Panigrahi, S. P., et al. (2025). CNT/Graphene reinforced PLA-based composites via FDM. Results in Engineering, 25, 104472.

[17] Bilkar, D., Keshavamurthy, R., & Tambrallimath, V. (2019). Carbon nanofiber reinforced polymer composites via FDM. Materials Today: Proceedings, 46, 4559–4562.

[18] Makannavar, R., Keshavamurthy, R., & Biradar, M. (2019). Graphite-filled ABS polymer composites via FDM. IOP Conference Series, 577, 012146.

[19] Deepak, J., Adarsha, H., Keshavamurthy, R., & Ramkumar, N. P. (2023). Friction and wear characteristics of additive manufactured CNT-reinforced HDPE composites. Tribology Transactions, 66(6), 1043–1056.

[20] Srinivasan, T., & Babu, V. S. (2020). Mechanical properties of SLA-printed polymer composites: A review. Journal of Manufacturing Processes, 56, 440–460.

[21] Wang, X., Zhao, L., & Fuh, J. Y. H. (2019). Effect of porosity on mechanical properties of 3D printed polymers: Experiments and micromechanical modeling based on X-ray computed tomography analysis. Polymers, 11(7), 1154.

[22] Ibrahim, Y., & Melenka, G. W. (2020). Review of fiber-reinforced polymer composites used in additive manufacturing. Polymer Composites, 41(1), 4–23.

[23] Ning, F., Cong, W., Qiu, J., Wei, J., & Wang, S. (2015). Additive manufacturing of carbon fiber reinforced thermoplastic composites using fused deposition modeling. Composites Part B: Engineering, 80, 369–378.

[24] Blok, L. G., Longana, M. L., Yu, H., & Woods, B. K. S. (2018). An investigation into 3D printing of fibre reinforced thermoplastic composites. Additive Manufacturing, 22, 176–186.

[25] Yao, T., Ye, J., Deng, Z., Zhang, K., Ma, Y., & Ouyang, H. (2020). Tensile failure strength and separation angle of FDM 3D printing PLA material: Experimental and theoretical analyses. Composites Part B: Engineering, 188, 107894.